Denudation partitioning in carbonate regions reveal climatic and tectonic drivers of carbonate landscape evolution

Richard Ott[1,2], Sean F. Gallen[3], David Helman[4,5]

[1]*Department of Earth Sciences, ETH Zurich, Zurich, Switzerland*

[2]*GFZ German Research Centre for Geosciences, Potsdam, Germany*

[3]*Department of Geosciences, Colorado State University, Fort Collins, US*

[4]*Department of Soil and Water Sciences, Institute of Environmental Sciences, Faculty of Agriculture, Food and Environment, Hebrew University of Jerusalem, Rehovot, Israel*

[5]*Advanced School for Environmental Studies, The Hebrew University of Jerusalem, Jerusalem, Israel*

ABSTRACT

Carbonate rocks are highly reactive and presumably have higher ratios of chemical weathering to total denudation relative to most other rock types. Their high chemical reactivity affects the first-order morphology of carbonate-dominated landscapes and their sensitivity to climate. However, there have been few efforts to quantify the partitioning of denudation into physical erosion and chemical weathering in carbonate landscapes such that their sensitivity to changing climate and tectonic conditions and its effect on topography remains elusive. Here, we compile bedrock and catchment-average cosmogenic calcite-^{36}Cl denudation rates and compare them to weathering rates. Local bedrock lowering and weathering rates are comparable, ~20 – 40 mm/ka, whereas catchment-average rates, which exist only for the Mediterranean, are ~2.7 times higher. This discrepancy is lower than the 15-fold difference in silicate-rich rocks illustrating that elevated weathering rates make denudation more spatially uniform in carbonate-dominated landscapes. Catchment-average denudation rates correlate well with topographic relief and hillslope gradient. Comparing these results with weathering rates shows that mechanical erosion processes contribute ~50% of denudation in southern France and ~70% in Greece and Israel. Our results indicate that the partitioning between largely slope-independent chemical weathering and slope-dependent mechanical erosion varies based on climate and tectonics. In humid, slowly uplifting regions, carbonates are associated with low-lying, flat topography because slope-independent chemical weathering dominates denudation. In contrast, in more arid climates with rapid rock uplift rates, carbonate rocks form steep mountains that facilitate rapid, slope-dependent mechanical erosion required to compensate for inefficient chemical weathering coupled with runoff loss to groundwater systems.

INTRODUCTION

Landscapes denude through a combination of mechanical erosion processes and chemical weathering. In most silicate-rich landscapes, erosion is the dominant denudation process. In contrast, carbonates are more susceptible to chemical weathering, likely resulting in a different partitioning of denudation into erosion and weathering for the same climatic and tectonic conditions. These differences in denudation partitioning should have pronounced effects on landscape morphology, presumably making carbonate landscapes more sensitive to differences in climate. However, few studies have quantified the relative contributions of erosion and weathering to denudation in carbonate-dominated landscapes, the effect of climate and tectonics on such partitioning, and its impact on topography.

The limited number of studies investigating denudation partitioning in carbonates stems largely from challenges in quantifying long-term mechanical erosion. Solution fluxes from dissolved loads and direct outcrop measurements with limestone tablets have been used extensively to quantify limestone weathering rates (Plan, 2005; Calmels et al., 2014). Recent advances in cosmogenic ^{36}Cl production rate calibration and calculation (Schimmelpfennig et al., 2009; Marrero et al., 2016b) now allow for accurate calculation of total denudation rates in carbonates at the outcrop and catchment scale. Through the comparison of cosmogenic radionuclide (CRN) measurements with weathering rates, it is possible to isolate the contribution of mechanical erosion by subtracting weathering from total denudation rates (Ott et al., 2019), provided that the disparate integration timescales of each measurement have a negligible impact on measurement comparisons, and if CRN weathering biases can be accounted for (Ott et al., 2022).

Studies applying some combination of these techniques have arrived at different conclusions regarding denudation in carbonates. Several recent studies assumed that the effects of mechanical rock removal are negligible (Ryb et al., 2014a, 2014b; Avni et al., 2018), implying chemical weathering dominates carbonate denudation budgets. However, other studies found that mechanical processes likely play a critical role in carbonate denudation (Newson, 1971; Covington et al., 2015; Thomas et al., 2017; Ben-Asher et al., 2021). Here, we contribute to this growing effort by compiling and comparing available cosmogenic calcite-^{36}Cl denudation rate measurements with catchment average weathering rates collected from the same areas to quantify the partitioning between mechanical and chemical surface lowering in carbonate terrains across climatic and tectonic gradients. We use this analysis to illuminate how denudation partitioning varies as a function of climate and tectonics and highlight that carbonate regions are more susceptible to climate-topography interactions than silicate-rich rocks.

METHODS

^{36}Cl denudation rate compilation

We compiled 232 bedrock and 43 fluvial sediment ^{36}Cl measurements from the literature to determine denudation rates at the outcrop and catchment scale, respectively (Fig.1, Tab. S1). The bedrock denudation rates were sampled from bedrock outcrops or amalgamated clasts on hillslopes or ridgetops and thus record local bedrock lower rates. In contrast, the alluvial sediment samples are assumed to be well-mixed and provide an average denudation rate across the upstream drainage area. ^{36}Cl denudation rate calculation requires knowledge of the chemical composition of the host rock and the target mineral analyzed (Schimmelpfennig et al., 2009). To compare denudation rates from different studies, we compiled all chemical sample data from the literature or, if unavailable, contacted the authors and recalculated all denudation rates with

CRONUScalc v2.1 (Marrero et al., 2016a) (Tab. S1). Ott et al. (2022) showed that weathering can bias CRN measurements of soluble target minerals such as calcite, but tests with weathering corrections show that this effect is negligible for the samples considered here, therefore, we present the uncorrected denudation rates (see supplement).

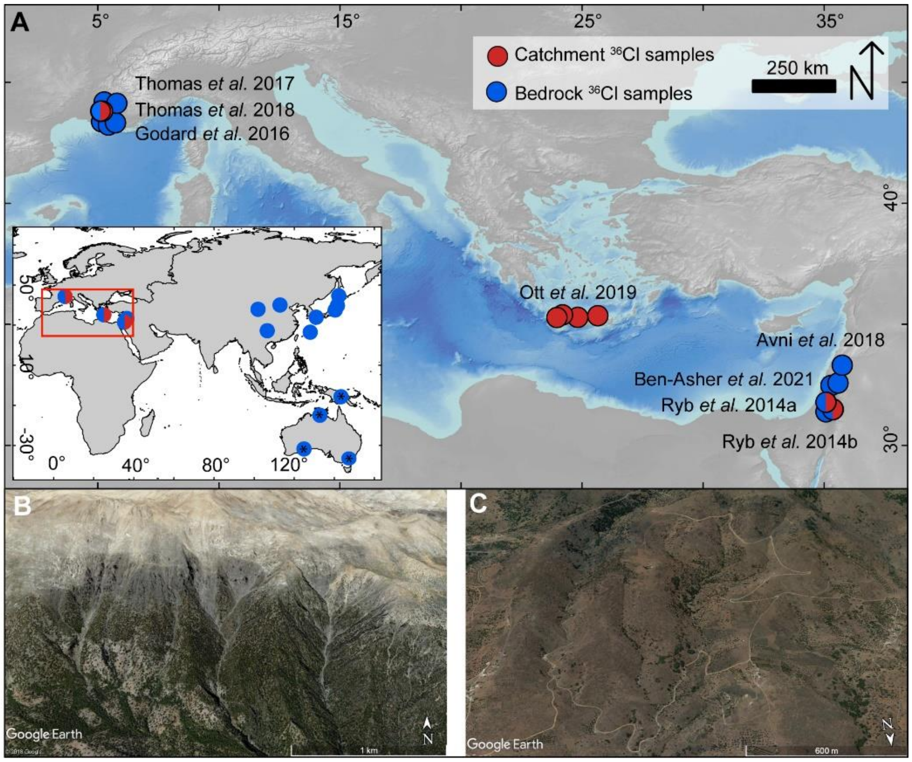

*Fig. 1: (A) Location of ^{36}Cl denudation rate measurements compiled for this study in the Mediterranean and globally (inset). *samples not included due to lack of location and compositional data. (B) Typical carbonate catchment in the Lefka Ori range on Crete, Greece, with partial forest cover and small landslide scars. (C) Typical low relief catchment on Crete.*

Carbonate weathering rate calculations

We calculated carbonate weathering rates for areas of published catchment-average denudation rates to infer the rates of landscape-scale mechanical erosion. Erosion can be assumed to equal denudation minus weathering because, despite deep solution features such as caves, the majority of carbonate dissolution takes place close to the Earth's surface (Gunn, 1981; Worthington and Smart, 2004). In southern France, we used time-averaged water data of [Ca^{2+}] and [Mg^{2+}] for springs and wells, provided from the national portal of water data (ADES) (Tab. S3). For the catchments in Israel, regional well and spring data were published by Ryb *et al.* (2014b), and in Crete, weathering rates were reported by Ott *et al.* (2019). Water chemistry data were used in conjunction with satellite-derived averages of precipitation and actual evapotranspiration (AET) to calculate carbonate weathering rates following the approach of Ott *et al.* (2019) (see supplement, Tab. S4).

RATES OF CARBONATE DENUDATION

Bedrock denudation rates and weathering rates calculated from water data are similar and generally fall between 20 - 40 mm/ka (mean: 29 and 32 mm/ka, respectively) (Fig. 2). The similarity of lowering rates for outcrops and weathering suggests that weathering is the dominant denudation process for exposed bedrock on hillslopes. Correlations between bedrock denudation rate and topographic and climatic variables are weak ($r^2 < 0.26$) (Fig. S2). While region-specific bedrock denudation rates show positive relationships with mean annual precipitation (MAP) (Fig. 2D), the strong covariation of topography and precipitation (Fig. S3) does not allow isolating climatic effects from these data. Site-specific variations in bedrock lithology, soil cover versus bare bedrock, and geomorphic sampling position likely contribute to the data scatter. Thus, our further analysis focuses primarily on the alluvial samples.

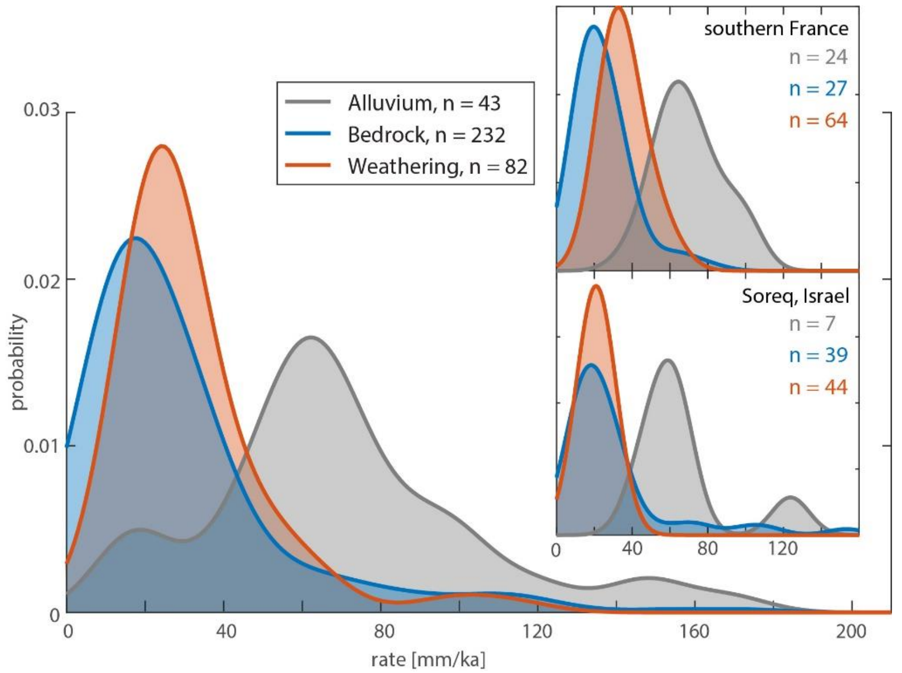

Fig. 2: (A) Kernel density plot of weathering, bedrock and alluvial denudation rates in carbonate catchments for all compiled data. (B) & (C) The same plots for southern France and the Soreq catchment in Israel.

Catchment-average denudation rates from alluvial samples are consistently higher (mean 81 mm/ka; 2.7 times higher) than bedrock denudation and weathering rates (Fig. 2). Discrepancies between bedrock and alluvial denudation rates have been interpreted as reflecting growing topographic relief (Small and Anderson, 1998; Hancock and Kirwan, 2007; Thomas et al., 2017), or higher weathering rates below soil-covered bedrock and therefore a sampling bias toward fresh outcrop surfaces (Portenga and Bierman, 2011). However, it is unlikely that all studies comparing bedrock-interfluve samples and catchment averages would find increasing relief. If the rate discrepancy is due to soil cover, measured soil production rates should equal the catchment-average rates. Yet, a global compilation of soil production rates shows that most measurements are significantly lower than the catchment-average denudation rates (Heimsath et al., 2012). An alternative explanation is that the bedrock denudation and soil production rates, whether in carbonates or siliciclastic rocks, represent a biased sampling of stable portions of the landscape (e.g., areas not affected by recent mass-wasting). Catchment-average sampling incorporates all portions of the upstream landscape and reflects a mix between the locally high denudation rate associated with mass wasting and a “background” rate set by bedrock denudation and soil production.

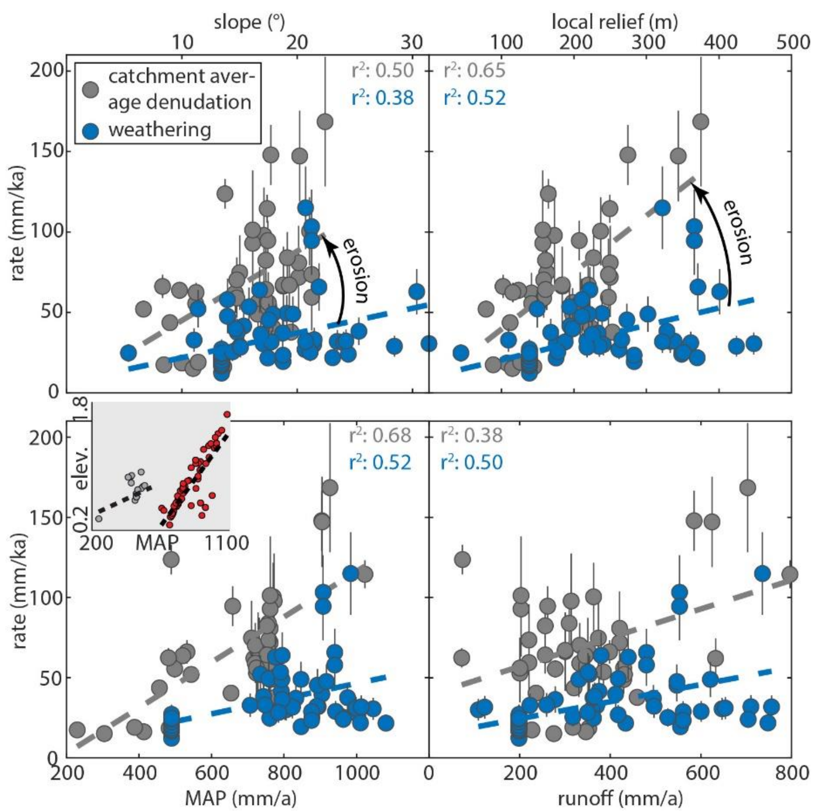

Fig. 3: Correlations between catchment average ^{36}Cl denudation rates, carbonate weathering rates, and topographic and climatic metrics. Inset-C: Correlation between MAP and elevation illustrating orographic precipitation in the analyzed areas (Israel, grey; France and Crete, red).

MECHANICAL DENUDATION IN CARBONATE LANDSCAPES

There are three explanations for the two-to three-fold difference between catchment-scale weathering rates and basin-average denudation rates: (1) Catchment-average rates overestimate denudation due to low CRN concentration material from deep (> 5 m, Yanites *et al*., 2009) landslides; (2) higher effective precipitation earlier in the averaging time window of CRNs (Ryb et al., 2014b, 2015); (3) mechanical denudation of carbonates. The deep-seated landslide bias seems unlikely due to the consistent discrepancy between catchment average denudation and weathering in a diverse array of topography, from low relief and slope areas in Israel to the rugged mountainous terrain of Crete (Fig. 1). Furthermore, most sampled catchments drain moderately sized areas (10’s of km^2) and are therefore large enough to buffer potential biases arising from mass-wasting (Niemi et al., 2005; Yanites et al., 2009).

The disparate integration timescales of CRNs (10^2– 10^5 yrs) and weathering rate measurements (0 – 10^2 yrs) (Plummer et al., 2001) lead Ryb *et al.* (2014b; 2015) to suggest that higher CRN denudation rates integrated a history of more vigorous weathering associated with past wetter climates. Most catchment-average rates integrate from modern to mid-Holocene, with the lowest rates integrating until the last glacial maximum (LGM). To test this hypothesis, we compared modern precipitation to 1 km resolution WorldClim paleo-precipitation maps from three different climate models (Fick and Hijmans, 2017). We found that mid-Holocene precipitation in all three Mediterranean sampling areas is predicted to have been between 2 and 27% higher in the mid-Holocene and between 25% drier or 55% wetter for the LGM depending on the area and preferred model (Tab. S4). Since weathering scales linearly with the water availability (White, 1984), these changes in precipitation, even with a total drawdown of AET, cannot explain the data discrepancy through an increased paleo-water flux when integrated over time.

Catchment-average denudation rates show strong-to-moderate correlations with topographic metrics such as local relief and slope (Fig. 3A, B). Catchment-average rates also scale strongly with precipitation, however, all study sites exhibit orographic precipitation such that precipitation is correlated with topography (Figs. 3C, S3). When comparing denudation rates to runoff, the correlation is weak, and slopes of the regression lines for catchment average denudation and weathering rate are similar (Fig. 3D). Weathering rates correlate weakly-to-moderately with topographic and climatic variables but remain consistently lower than catchment-average denudation rates across all variable gradients. Collectively, these observations suggest that in Mediterranean carbonate landscapes, mechanical erosion contributes significantly to denudation because (1) catchment average denudation rates are substantially higher than weathering rates, (2) denudation scales with topographic steepness, (3) the difference between denudation and weathering, which we interpret as erosion, also increases with increasing topographic steepness, whereas (4) the increase of denudation with runoff can be fully accounted for by an increase in weathering (Fig. 3D).

LANDSCAPE EVOLUTION IN CARBONATES COMPARED TO OTHER ROCK TYPES

The trend of higher carbonate catchment-average rates compared to bedrock lowering rates is consistent with ^{10}Be measurements from siliciclastic units where basin denudation rates are ~15 times higher than average outcrop lowering rates (Portenga and Bierman, 2011). The smaller ~2.7-fold discrepancy between local bedrock and catchment-average rates in carbonate terrains is best explained by the elevated role of chemical weathering in carbonates (~ 1/3 of denudation, Fig. 3) compared to silica-rich rocks (< 5% of denudation) (Larsen et al., 2014). These findings have important implications for landscape evolution in carbonates and their topographic response to tectonic uplift and climate because mechanical erosion is slope-dependent, whereas weathering mostly depends on climate and vegetation.

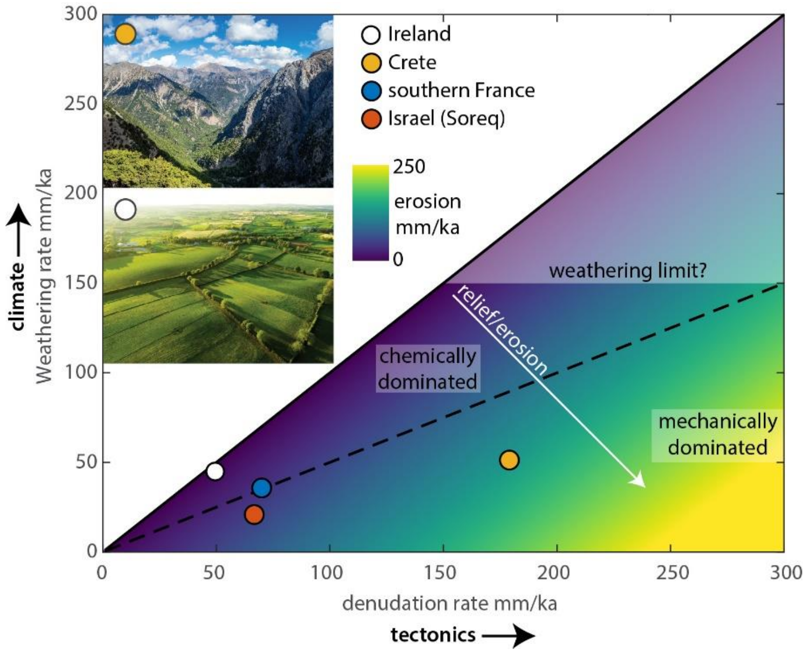

Fig. 4: Mean weathering versus mean denudation rates for the sites with alluvial denudation data. We added Ireland as an example of a region dominated by chemical weathering processes (Simms, 2004) with rates by Drew (2001). Chemical weathering dominated landscapes will be subdued (white dot, southern Ireland); high erosion rates will lead to high relief areas dominated by slope-dependent mechanical processes (yellow dot, Crete).

Averaging catchment denudation and weathering rates for southern France, Israel (Soreq), and Crete, we find erosion-to-weathering ratios of 1.0, 2.2, and 2.5, respectively (Fig. 4). The substantial amount of mechanical erosion in these carbonate landscapes requires steep, high relief topography allowing slope-dependent processes to thrive. Carbonates in slowly uplifting areas will denude sluggishly, and under favorable climatic conditions, weathering alone is sufficient to balance rock uplift with negligible mechanical erosion. In such a case, a carbonate landscape will remain subdued, and less-soluble lithologies will stick out because surface-lowering can only be achieved through erosion requiring local slopes to form. This can be observed in Ireland, where carbonates denude mostly through dissolution, and eroding sandstone ridges form the topographic highs (Simms, 2004).

The weathering rate will mostly be set by local climate but may be subject to a dissolution speed limit because (1) of a chemical threshold of <200 mg/l water hardness, which has been observed globally (Covington et al., 2015; Gaillardet et al., 2018), (2) an increase in precipitation will typically be partially compensated by an increase in AET, and (3) tropical regions with high runoff have lower water hardness due to a decrease in carbonate solubility with temperature. A global compilation of carbonate weathering rates finds a maximum rate of ~140 mm/ka (Gaillardet et al., 2018), similar to our highest rate of 115 mm/ka. These rates may represent a carbonate weathering speed limit beyond which mechanical erosion becomes dominant, and topography steepens (Fig. 4).

In carbonate regions where mechanical erosion prevails, surface water infiltration will lower the discharge of surface streams. Reduction in stream discharge will decrease the erosional efficiency and cause steepening of the landscape compared to regions with less-soluble bedrock (Ott et al., 2019). This explains why carbonate terrain in locations with arid to semi-arid climate and significant uplift rates form steeper topography than areas underlain by silicate-rich lithologies (Ott et al., 2019; Ott, 2020), and carbonates form the low parts of the landscape, e.g. in Ireland or the Appalachians, where uplift rates are low, and the climate is favorable for weathering. Hence, the topography of carbonate regions is more sensitive to the interplay of tectonics and climate compared to silicate-rich rocks. Studies investigating the climatic and tectonic effects on topography typically report that tectonics govern the first-order landscape morphology (Seybold et al., 2021). In contrast, we argue that carbonate regions offer the potential to observe strong controls of climate and highly non-linear responses to tectonics on landscape evolution.

ACKNOWLEDGMENTS

R.O. was funded by Marie Curie actions grant number 674899 and Swiss National Science Foundation grant number P2EZP2_191866. S.F.G. was partially supported by NSF award EAR-204190 and funds provided by Colorado State University.

REFERENCES CITED

Avni, S., Joseph-Hai, N., Haviv, I., Matmon, A., Benedetti, L., and Team, A., 2018, Patterns and rates of 103−105 yr denudation in carbonate terrains under subhumid to subalpine climatic gradient, Mount Hermon, Israel: GSA Bulletin, v. 131, p. 899–912, doi:10.1130/B31973.1.

Ben-Asher, M., Haviv, I., Crouvi, O., Roering, J.J., and Matmon, A., 2021, The convexity of carbonate hilltops: 36Cl constraints on denudation and chemical weathering rates and implications for hillslope curvature: GSA Bulletin, doi:10.1130/b35658.1.

Calmels, D., Gaillardet, J., and François, L., 2014, Sensitivity of carbonate weathering to soil CO 2 production by biological activity along a temperate climate transect: Chemical Geology, v. 390, p. 74–86, doi:10.1016/j.chemgeo.2014.10.010 S1 - 13.

Covington, M.D., Gulley, J.D., and Gabrovšek, F., 2015, Natural variations in calcite dissolution rates in streams: Controls, implications, and open questions: Geophysical Research Letters, v. 42, p. 2836–2843, doi:10.1002/2015GL063044.

Drew, D.P., 2001, Classic Landforms of the Burren Karst: Sheffield, Geographical Association and the British Geomorphological Research Group, 52 p.

Fick, S.E., and Hijmans, R.J., 2017, WorldClim 2: new 1-km spatial resolution climate surfaces for global land areas: International Journal of Climatology, v. 37, p. 4302–4315, doi:10.1002/joc.5086.

Gaillardet, J., Calmels, D., Romero-Mujalli, G., Zakharova, E., and Hartmann, J., 2018, Global climate control on carbonate weathering intensity: Chemical Geology, doi:10.1016/j.chemgeo.2018.05.009.

Gunn, J., 1981, Limestone solution rates and processes in the Waitomo District, New Zealand: Earth Surface Processes and Landforms, v. 6, p. 427–445, doi:10.1002/esp.3290060504.

Hancock, G., and Kirwan, M., 2007, Summit erosion rates deduced from 10Be: Implications for relief production in the central Appalachians: Geology, v. 35, p. 89, doi:10.1130/G23147A.1.

Heimsath, A.M., DiBiase, R.A., and Whipple, K.X., 2012, Soil production limits and the transition to bedrock-dominated landscapes: Nature Geoscience, v. 5, p. 210–214, doi:10.1038/ngeo1380.

Larsen, I.J., Montgomery, D.R., and Greenberg, H.M., 2014, The contribution of mountains to global denudation: Geology, v. 42, p. 527–530, doi:10.1130/G35136.1.

Marrero, S.M., Phillips, F.M., Borchers, B., Lifton, N., Aumer, R., and Balco, G., 2016a, Cosmogenic nuclide systematics and the CRONUScalc program: Quaternary Geochronology, v. 31, p. 160–187, doi:10.1016/j.quageo.2015.09.005.

Marrero, S.M., Phillips, F.M., Caffee, M.W., and Gosse, J.C., 2016b, CRONUS-Earth cosmogenic 36 Cl calibration: Quaternary Geochronology, v. 31, p. 199–219, doi:10.1016/j.quageo.2015.10.002.

Newson, M.D., 1971, A Model of Subterranean Limestone Erosion in the British Isles Based on Hydrology: Transactions of the Institute of British Geographers, v. 54, p. 55, doi:10.2307/621362.

Niemi, N.A., Oskin, M., Burbank, D.W., Heimsath, A.M., and Gabet, E.J., 2005, Effects of bedrock landslides on cosmogenically determined erosion rates: Earth and Planetary Science Letters, v. 237, p. 480–498, doi:10.1016/j.epsl.2005.07.009.

Ott, R.F., 2020, How Lithology Impacts Global Topography, Vegetation, and Animal Biodiversity: A Global-Scale Analysis of Mountainous Regions: Geophysical Research Letters, v. 47, doi:10.1029/2020GL088649.

Ott, R.F., Gallen, S.F., Caves-Rugenstein, J.K., Ivy-Ochs, S., Helman, D., Fassoulas, C., Vockenhuber, C., Christl, M., and Willett, S.D., 2019, Chemical versus mechanical denudation in meta-clastic and carbonate bedrock catchments on Crete, Greece, and mechanisms for steep and high carbonate topography: Journal of Geophysical Research Earth Surface, doi:10.1029/2019JF005142.

Ott, R.F., Gallen, S.F., and Granger, D.E., 2022, Cosmogenic nuclide weathering biases: Corrections and potential for denudation and weathering rate measurements: Geochronology Discussions, doi:10.5194/gchron-2022-5.

Plan, L., 2005, Factors controlling carbonate dissolution rates quantified in a field test in the Austrian alps: Geomorphology, v. 68, p. 201–212, doi:10.1016/j.geomorph.2004.11.014.

Plummer, L.N., Busenberg, E., Böhlke, J.K., Nelms, D.L., Michel, R.L., and Schlosser, P., 2001, Groundwater residence times in Shenandoah National Park, Blue Ridge Mountains, Virginia, USA: a multi-tracer approach: Chemical Geology, v. 179, p. 93–111, doi:10.1016/S0009-2541(01)00317-5.

Portenga, E.W., and Bierman, P.R., 2011, Understanding Earth's eroding surface with 10Be: GSA Today, v. 21, p. 4–10, doi:10.1130/G111A.1.

Ryb, U., Matmon, A., Erel, Y., Haviv, I., Benedetti, L., and Hidy, A.J., 2014a, Styles and rates of long-term denudation in carbonate terrains under a Mediterranean to hyper-arid climatic gradient: Earth and Planetary Science Letters, v. 406, p. 142–152, doi:10.1016/j.epsl.2014.09.008.

Ryb, U., Matmon, A., Erel, Y., Haviv, I., Katz, A., Starinsky, A., Angert, A., and Team, A., 2014b, Controls on denudation rates in tectonically stable Mediterranean carbonate terrain: GSA Bulletin, v. 126, p. 553–568, doi:10.1130/B30886.1.

Ryb, U., Matmon, A., Haviv, I., and Benedetti, L., 2015, Exhumation and uplift coupled with precipitation along the western Dead Sea Rift margin: Geology, v. 43, p. 483–486, doi:10.1130/G36331.1.

Schimmelpfennig, I., Benedetti, L., Finkel, R., Pik, R., Blard, P.H., Bourlès, D., Burnard, P., and Williams, A., 2009, Sources of in-situ 36Cl in basaltic rocks. Implications for calibration of production rates: Quaternary Geochronology, v. 4, p. 441–461, doi:10.1016/j.quageo.2009.06.003.

Seybold, H., Berghuijs, W.R., Prancevic, J.P., and Kirchner, J.W., 2021, Global dominance of tectonics over climate in shaping river longitudinal profiles: Nature Geoscience 2021, p. 1–5, doi:10.1038/s41561-021-00720-5.

Simms, M.J., 2004, Tortoises and hares: Dissolution, erosion and isostasy in landscape evolution: Earth Surface Processes and Landforms, v. 29, p. 477–494, doi:10.1002/esp.1047.

Small, E.E., and Anderson, R.S., 1998, Pleistocene relief production in Laramide mountain ranges, western United States: Geology, v. 26, p. 123, doi:10.1130/0091-7613(1998)026<0123:PRPILM>2.3.CO;2.

Thomas, F. et al., 2017, Morphological controls on the dynamics of carbonate landscapes under a mediterranean climate: Terra Nova, v. 29, p. 173–182, doi:10.1111/ter.12260.

White, W.B., 1984, Rate processes: chemical kinetics and karst landform development, *in* La Fleur ed., Groundwater as a geomorphic agent, Allen and Unwin, p. 227–248.

Worthington, S.R.H., and Smart, C.C., 2004, Groundwater in karst: conceptual models, *in* Gunn, J. ed., Encyclopedia of Caves and Karst Science, Fitzroy Dearborn, p. 399–401.

Yanites, B.J., Tucker, G.E., and Anderson, R.S., 2009, Numerical and analytical models of cosmogenic radionuclide dynamics in landslide-dominated drainage basins: Journal of Geophysical Research, v. 114, p. 12857, doi:10.1029/2008JF001088.

Supplemental material - Denudation partitioning in carbonate regions reveal climatic and tectonic drivers of carbonate landscape evolution

Richard Ott[1,2], Sean F. Gallen[3], David Helman[4,5]

[1]*Department of Earth Sciences, ETH Zurich, Zurich, Switzerland*

[2]*GFZ German Research Centre for Geosciences, Potsdam, Germany*

[3]*Department of Geosciences, Colorado State University, Fort Collins, US*

[4]*Department of Soil and Water Sciences, Institute of Environmental Sciences, Faculty of Agriculture, Food and Environment, Hebrew University of Jerusalem, Rehovot, Israel*

[5]*Advanced School for Environmental Studies, The Hebrew University of Jerusalem, Jerusalem, Israel*

This supplement includes a description of the carbonate dissolution rate calculation, the estimation of actual evapotranspiration, ^{36}Cl weathering bias correction, and the calculation of topographic metrics. Moreover, it includes the ^{36}Cl denudation rate compilation and water chemistry data used for southern France. Supplementary figures show correlations between bedrock lowering and topographic and climatic metrics. We also show the estimated recharge areas used for carbonate dissolution rate calculation and a p-value matrix for the significance of our correlations.

Carbonate dissolution rate calculation

All chemical data were corrected for precipitation input by assuming that all $[Cl^-]$ is derived from precipitation, and that other cations are scaled by seawater ratios (Stallard and

Edmond, 1981). Water data from Israel were not corrected due to unknown [Cl^-]; however, the correction for [Ca^{2+}] was usually < 1% and is therefore assumed to be negligible.

To calculate the water flux, we used satellite-derived precipitation and actual evapotranspiration data (AET). Precipitation was derived from the WorldClim 1 km dataset (Fick and Hijmans, 2017) and averaged for each catchment. To determine the runoff available for dissolution, AET was estimated from a parameterization of vegetation indices (PaVI-E) model (Helman et al., 2015) using MODerate resolution Imaging Spectroradiometer (MODIS) satellite data from 2000 to 2016 at 1 km resolution and water vapor flux data from the eddy covariance tower international net (FLUXNET) (see description below for details). The dissolution rate is then calculated by assuming that all [Ca^{2+}] and [Mg^{2+}] in the water are derived from carbonate dissolution and using the water flux from our local runoff calculation for each catchment. A recharge area for runoff averaging was estimated for groundwater water samples based on surface topography and local geology (see Fig. S1 for estimated groundwater recharge areas).

Dissolution rates were calculated with an uncertainty of 10% on the precipitation data and 20% on the actual evapotranspiration. Because recharge areas of springs and wells in karstic terrains can deviate significantly from topographically estimated areas (Fig. S1), we show a second estimate based on the P and AET average of the entire mountain range where the spring or well is located (Tab. S3). However, the difference in the average dissolution rate between both approaches is < 3%, and we, therefore, choose to use the topographic recharge area estimates outlined in Fig. S1.

Estimation of actual evapotranspiration

Actual evapotranspiration (AET) was calculated on a yearly basis at a 1 km spatial resolution using an empirical model (PaVI-E) based on relationships found between satellite-derived vegetation indices and eddy covariance fluxes (Helman et al., 2015). The advantage of PaVI-E is its independence of meteorological data, which avoids parameter dependency issues in climate-related studies.

PaVI-E was successfully validated against basin-scale AET derived from water balance calculations (i.e., AET= P – Q) in the Eastern Mediterranean region ($R^2 = 0.85$, $p<0.05$) and was shown to be comparable with other well-established physically-based AET models (Helman et al., 2015, 2017a). It has been used to study climate change impacts on the terrestrial water cycle and is considered a reliable tool for water balance calculations (Helman et al., 2017c, 2017b).

Topographic metric calculation

Topographic metrics were measured on a 1 arc-second (~30 m) Shuttle Radar Topography Mission dataset. Slope, mean elevation, mean slope, and mean local relief (500 m radius) were calculated using TopoToolbox (Schwanghart and Scherler, 2014).

Weathering corrections for denudation rates

Chemical weathering can bias cosmogenic nuclide-derived denudation rates. Regolith weathering can overestimate ^{36}Cl denudation rates because the soluble target mineral calcite may have a shorter regolith residence time than the bulk rock due to its high solubility. We use the methods proposed by Ott et al. (2022) to correct all alluvial denudation rates for regolith weathering. The correction requires knowledge of the regolith or bedrock composition. In the absence of direct bedrock compositional data, we use the reported bulk chemical composition of the samples as an estimate of regolith composition. We multiply the weight-percent CaO by 1.4 to estimate the calcite fraction in the regolith, take the SiO_2 weight-percent as fraction quartz, and assign the remainder as other insoluble minerals.

Additionally, we use the mean weathering rates for every area (Israel: 21 ± 3 mm/ka, Crete: 48 ± 11 mm/ka, France: 37 ± 8 mm/ka) for the corrections. On Crete, we estimate 30 cm regolith thickness within the sampled catchments from the European soil database (ESDAC) (Panagos et al., 2012). We use this thickness in conjunction with a density of 1.5 g/cm^3 to derive a soil mass of 45 g/cm^2. The same value is found in southern France, with soil depth estimated from the maps of Chen et al. (2019). For the Soreq catchment in Israel, Ryb et al. (2014) report regolith thicknesses between 0 and 75 cm. We take the middle (37.5 cm) and use it with the reported regolith density of 1.4 g/cm^3 to derive an average soil mass of 52.5 g/cm^2.

Weathering-corrected denudation rates are similar to conventional denudation rates, with a maximum difference of about 7%. The sample compositions reported from southern France indicate almost pure limestone. Therefore, the bias for these rocks is very small. The WeCode package by Ott (2022) used for weathering corrections does not account for radioactive decay. This explains why the weathering-corrected denudation rates from southern France are marginally higher than the conventional rates, including decay. For five samples, the weathering correction could not be applied because the reported nuclide concentration was greater than the theoretical maximum nuclide concentration for the provided parameter combination (N_{max}, for definition, see Ott et al., 2022). This is likely linked to uncertainties in the input parameters, such as weathering rate, regolith mass, etc. Likely, for some samples considered here, the actual catchment weathering rate is lower than the mean weathering rate for the area. However, the distribution of water sampling stations does not allow deriving weathering rates close to every location sampled for cosmogenic nuclides. In general, the weathering bias in the investigated samples is low due to the low weathering rates and clean limestone composition of many samples. Because the corrections are low and uncertainty exists in some of the correction parameters, we chose to report uncorrected denudation rates in the main text.

Tab. S2: Output of weathering correction calculation for denudation rates.

Location	**Sample**	**Denudation rate mm/ka**	**err**	**Conventional denudation rate mm/ka**	**Rate difference %**
Crete	Cl-617-2	87.3	7.0	93.8	6.9
Crete	Cl-617-3				rate could not be calculated because N > Nmax
Crete	Cl-617-6	108.5	5.4	111.9	3.0
Crete	Cl-617-8	159.8	22.5	166.0	3.7
Crete	Cl-617-10	141.5	9.5	146.0	3.0
Crete	Cl-617-15	142.0	13.4	144.7	1.9
Crete	WC-616-8	521.5	117.1	531.8	1.9
France	BRO1B-G	63.0	11.5	62.2	-1.1
France	ORM01B-G			37.8	rate could not be calculated because N > Nmax
France	ORM02B-G	72.6	23.4	72.0	-0.8
France	ORM02B-S	81.7	21.7	80.9	-0.9
France	ORM03B-G	67.1	23.3	66.5	-1.0
France	ORM03B-S	67.9	20.5	67.2	-1.0
France	PLBS-1G	56.4	8.0	56.1	-0.4
France	PLBS-1S			48.9	rate could not be calculated because N > Nmax
France	PLBS-2S	53.9	7.3	53.7	-0.3
France	PLBS-3G	100.7	19.8	100.6	-0.1
France	PLBS-4G	84.4	14.7	84.1	-0.4
France	PLS-E1	67.4	19.3	67.2	-0.3
France	PLS-E2	75.1	22.1	74.9	-0.2
France	REC01B-S	98.3	28.1	97.9	-0.4
France	REC02B-G	93.3	28.1	93.1	-0.3
France	REC02B-S	101.8	35.0	101.4	-0.4
France	ROQ01B-G	59.7	11.3	59.1	-1.0
France	ROQ01B-S	70.8	12.8	70.4	-0.6
France	TAP01B-G	60.0	19.6	59.5	-0.9
France	TAP01B-S	74.1	21.0	73.6	-0.6
France	TAP02B-G	53.5	17.4	53.0	-1.0
France	TAP02B-S	56.6	17.9	56.2	-0.8
France	VID01B-S	64.7	10.6	64.3	-0.7
France	VID02B-S	82.5	15.3	82.1	-0.5
Israel/Soreq	SQSED1			41.5	rate could not be calculated because N > Nmax
Israel/Soreq	SQSED2	60.8	1.4	63.4	4.1
Israel/Soreq	SQSED3	59.6	1.3	61.1	2.5

Israel/Soreq	SQSED4	117.3	5.3	118.7	1.1
Israel/Soreq	SQSED5	50.5	0.4	53.1	4.9
Israel/Soreq	SQSED6	58.6	1.2	59.9	2.1
Israel/Soreq	SQSED7			49.8	rate could not be calculated because N > Nmax

Tab S3: Raw and precipitation corrected water data from southern France. [Ca^{2+}] and [Mg^{2+}]. n – number of samples, min – minimum concentration, max – maximum concentration measured.

National Code of station	Area	Lon	Lat	Ca					Mg					Cl			
				n	min	max	average	corrected	n	min	max	average	corrected	n	min	max	average
09678X0109/HY	Luberon	5.3802	43.8203	1	91.8	91.8	91.8	91.7	1	3.4	3.4	3.4	3.1	1	5.1	5.1	5.1
09685X0011/F	Luberon	5.4057	43.8285	5	77.0	85.2	80.9	80.8	5	6.5	8.7	7.6	7.3	10	3.7	4.8	4.5
09681X0069/FO	Luberon	5.4622	43.8399	2	102.4	110.0	106.2	106.0	2	3.4	3.5	3.5	2.7	2	10.1	11.4	10.8
09685X0013/F	Luberon	5.4171	43.7862	3	80.0	93.5	87.2	87.1	3	1.3	1.5	1.4	1.0	3	6.1	6.5	6.3
09685X0012/HY	Luberon	5.4226	43.7868	3	82.8	88.9	86.2	86.2	3	4.9	6.3	5.8	5.7	3	0.8	1.4	1.0
09674X0089/F	Luberon	5.3852	43.8361	3	68.0	74.0	70.7	70.4	3	2.6	3.5	3.0	2.1	3	13.9	14.9	14.3
09686X0019/F	Luberon	5.5380	43.7930	31	104.0	123.0	112.7	112.6	31	7.0	9.5	8.1	7.8	31	4.1	8.0	5.1
09676X0053/P	Luberon	5.1791	43.7531	7	55.0	120.0	103.4	102.9	7	4.4	16.1	13.5	11.8	8	10.7	31.0	25.7
09175X0016/HY	Lure	5.7888	44.1090	3	49.0	53.5	50.8	50.8	3	0.5	0.5	0.5	0.3	18	0.8	9.2	2.3
09431X0010/HY	Lure	5.8374	44.0668	5	46.0	65.5	59.4	59.3	5	0.5	1.5	1.0	0.8	24	2.3	9.2	3.3
09176X0008/TX	Lure	5.8944	44.1311	3	61.0	65.6	63.9	63.8	3	9.2	10.8	9.9	9.6	4	2.5	6.1	4.1
09431X0013/HY	Lure	5.7859	44.0506	1	87.0	87.0	87.0	86.9	1	1.9	1.9	1.9	1.6	6	3.8	5.1	4.3
09424X0015/HY	Lure	5.7059	44.0956	1	62.0	62.0	62.0	62.0	1	1.5	1.5	1.5	1.4	5	1.0	3.1	2.1
09153X1005/HY	Ventoux	5.2895	44.1881	4	56.6	65.0	61.1	61.0	4	3.7	4.1	3.8	3.6	4	2.4	3.1	2.7
09153X1004/HY	Ventoux	5.2734	44.2056	1	56.1	56.1	56.1	56.1	1	8.6	8.6	8.6	8.5	1	1.2	1.2	1.2
09154X1004/SO	Ventoux	5.3148	44.1923	3	57.2	64.0	59.5	59.5	3	1.9	2.3	2.2	2.0	3	2.1	2.5	2.3
09157X0014/HY	Ventoux	5.2233	44.1895	7	49.0	51.9	50.0	50.0	7	1.2	1.4	1.3	1.2	7	2.0	2.4	2.3
09165X1006/HY	Ventoux	5.4139	44.1248	8	73.0	85.0	77.8	77.7	8	5.1	7.5	6.2	6.0	8	2.8	3.9	3.3
09156X0074/F	Ventoux	5.2071	44.1833	8	64.5	70.4	67.0	67.0	8	1.4	2.1	1.7	1.5	9	1.9	2.4	2.2
10212X0020/HY	Sainte Victoire	5.5752	43.5188	3	60.6	139.6	89.1	88.6	3	5.5	27.6	13.2	11.8	3	17.0	27.9	21.1
10213X0051/P	Sainte Victoire	5.6411	43.5285	1	132.0	132.0	132.0	131.7	1	31.8	31.8	31.8	30.8	1	15.6	15.6	15.6
10213X0050/HY	Sainte Victoire	5.6422	43.5232	1	119.0	119.0	119.0	118.8	1	18.4	18.4	18.4	17.7	1	9.9	9.9	9.9
10213X0121/HY	Sainte Victoire	5.6013	43.5563	7	116.0	129.0	122.5	122.3	7	6.7	10.4	9.2	8.7	7	6.2	9.0	7.9
10451X0041/F	Sainte Baume	5.7711	43.3098	2	61.4	118.0	89.7	89.5	2	20.8	63.5	42.2	41.4	3	7.5	17.2	10.9
10444X0028/F	Sainte Baume	5.7559	43.3016	3	85.3	108.0	93.2	92.9	3	44.2	54.9	50.4	49.3	3	11.3	22.0	15.6
10444X0026/DA	Sainte Baume	5.7099	43.2898	9	66.8	73.4	70.0	69.8	9	27.5	31.0	28.9	28.2	9	9.7	12.0	10.6
10443X0291/HY	Sainte Baume	5.6600	43.2911	14	60.4	78.8	72.2	72.0	14	17.2	21.9	19.0	18.4	14	7.6	10.2	8.7

Tab. S4: Dissolution rates calculated using estimated recharge areas from topography (Fig. S1) together with average P and AET values for the entire mountain range of the sampled spring, well or river.

						Estimated recharge areas			Mountain range averages		
Location	**Country**	**N [°]**	**E [°]**	**[Ca^{2+}]**	**[Mg^{2+}]**	**P [mm/a]**	**AET [mm/a]**	**Dissolution rate [mm/a]**	**P [mm/a]**	**AET [mm/a]**	**Dissolution rate [mm/a]**
Agur1	Israel	31.7207	34.9162	61	35				490	291	0.021 ± 0.005
Agur2	Israel	31.7241	34.9139	56	35				490	291	0.02 ± 0.004
Agur3	Israel	31.7074	34.9399	59	33				490	291	0.02 ± 0.004
Agur4	Israel	31.6842	34.9803	62	32				490	291	0.02 ± 0.004
Agur5	Israel	31.6796	34.9890	91	34				490	291	0.026 ± 0.006
Agur6	Israel	31.6796	35.0088	58	29				490	291	0.019 ± 0.004
Agur7	Israel	31.6789	35.0276	57	29				490	291	0.018 ± 0.004
Agur8	Israel	31.7116	35.0106	70	30				490	291	0.021 ± 0.005
EnKarem1	Israel	31.7795	35.1557	48	14				490	291	0.013 ± 0.003
EnKarem13	Israel	31.7434	35.1531	53	24				490	291	0.016 ± 0.004
EnKarem14	Israel	31.7986	35.1697	61	27				490	291	0.019 ± 0.004
EnKarem15	Israel	31.7877	35.1622	65	30				490	291	0.02 ± 0.005
EnKarem16	Israel	31.7447	35.1762	60	25				490	291	0.018 ± 0.004
EnKarem17	Israel	31.7422	35.1643	36	21				490	291	0.012 ± 0.003
EnKarem3	Israel	31.8002	35.1251	62	33				490	291	0.02 ± 0.005
EnKarem9	Israel	31.8052	35.1716	55	24				490	291	0.017 ± 0.004
Karem9+1	Israel	31.8052	35.1716	61	26				490	291	0.018 ± 0.004
Eshtaol1	Israel	31.7769	35.0103	68	37				490	291	0.022 ± 0.005
Eshtaol2a	Israel	31.7770	35.0126	66	39				490	291	0.023 ± 0.005
Eshtaol3	Israel	31.8155	35.0232	74	35				490	291	0.023 ± 0.005
Eshtaol4	Israel	31.7995	35.0120	85	38				490	291	0.026 ± 0.006
Eshtaol5	Israel	31.7772	35.0255	59	31				490	291	0.019 ± 0.004
Eshtaol6	Israel	31.8097	35.0151	85	37				490	291	0.026 ± 0.006
Eshtaol7	Israel	31.7681	35.0122	52	29				490	291	0.017 ± 0.004
Eshtaol8	Israel	31.8028	35.0189	65	29				490	291	0.02 ± 0.004
Eshtaol9	Israel	31.7892	35.0161	69	31				490	291	0.021 ± 0.005
Hartuv3	Israel	31.7605	35.0085	61	37				490	291	0.021 ± 0.005
Hartuv4	Israel	31.7505	35.0001	68	35				490	291	0.022 ± 0.005
Modieen1	Israel	31.8605	35.0330	80	40				490	291	0.026 ± 0.006
Modieen2	Israel	31.8505	35.0435	81	30				490	291	0.023 ± 0.005
Modieen3	Israel	31.8266	35.0307	66	29				490	291	0.02 ± 0.004
Modieen4	Israel	31.8402	35.0361	60	27				490	291	0.018 ± 0.004
Uriya2	Israel	31.7958	34.9491	58	36				490	291	0.02 ± 0.005
Uriya3	Israel	31.8005	34.9576	66	39				490	291	0.023 ± 0.005
Uriya4	Israel	31.8159	34.9178	76	44				490	291	0.026 ± 0.006
Uriya6	Israel	31.8016	34.9508	80	37				490	291	0.025 ± 0.006
Uriya7	Israel	31.7621	34.9643	77	37				490	291	0.024 ± 0.005
Uriya8	Israel	31.8252	34.9428	88	40				490	291	0.027 ± 0.006
Uriya9a	Israel	31.7950	34.9754	78	38				490	291	0.025 ± 0.006
09678X0109/HY	France	43.8203	5.3802	91.7	3.1	794	424	0.035 ± 0.008	773	433	0.032 ± 0.007

09685X0011/F	France	43.8285	5.4057	80.8	7.3	802	443	0.032 ± 0.007	773	433	0.03 ± 0.007
09681X0069/FO	France	43.8399	5.4622	106.0	2.7	833	337	0.054 ± 0.012	773	433	0.037 ± 0.008
09685X0013/F	France	43.7862	5.4171	87.1	1.0	806	697	0.01 ± 0.002	773	433	0.03 ± 0.007
09685X0012/HY	France	43.7868	5.4226	86.2	5.7	823	701	0.011 ± 0.003	773	433	0.032 ± 0.007
09674X0089/F	France	43.8361	5.3852	70.4	2.1	761	398	0.026 ± 0.006	773	433	0.025 ± 0.006
09686X0019/F	France	43.7930	5.5380	112.6	7.8	793	418	0.046 ± 0.01	773	433	0.041 ± 0.009
09676X0053/P	France	43.7531	5.1791	102.9	11.8	707	484	0.026 ± 0.006	725	445	0.033 ± 0.007
09175X0016/HY	France	44.1090	5.7888	50.8	0.3	1081	647	0.022 ± 0.005	923	500	0.022 ± 0.005
09431X0010/HY	France	44.0668	5.8374	59.3	0.8	962	644	0.019 ± 0.004	923	500	0.025 ± 0.006
09176X0008/TX	France	44.1311	5.8944	63.8	9.6	894	184	0.054 ± 0.012	923	500	0.032 ± 0.007
09431X0013/HY	France	44.0506	5.7859	86.9	1.6	975	613	0.032 ± 0.007	923	500	0.038 ± 0.008
09424X0015/HY	France	44.0956	5.7059	62.0	1.4	1004	586	0.027 ± 0.006	923	500	0.027 ± 0.006
09153X1005/HY	France	44.1881	5.2895	61.0	3.6	1046	399	0.042 ± 0.009	912	444	0.031 ± 0.007
09153X1004/HY	France	44.2056	5.2734	56.1	8.5	999	345	0.043 ± 0.01	912	444	0.031 ± 0.007
09154X1004/SO	France	44.1923	5.3148	59.5	2.0	942	342	0.037 ± 0.008	912	444	0.029 ± 0.006
09157X0014/HY	France	44.1895	5.2233	50.0	1.2	963	259	0.036 ± 0.008	912	444	0.024 ± 0.005
09165X1006/HY	France	44.1248	5.4139	77.7	6.0	904	493	0.035 ± 0.008	912	444	0.04 ± 0.009
09156X0074/F	France	44.1833	5.2071	67.0	1.5	891	394	0.034 ± 0.008	912	444	0.032 ± 0.007
10212X0020/HY	France	43.5188	5.5752	88.6	11.8	744	378	0.038 ± 0.008	738	366	0.038 ± 0.009
10213X0051/P	France	43.5285	5.6411	131.7	30.8	776	336	0.074 ± 0.017	738	366	0.063 ± 0.014
10213X0050/HY	France	43.5232	5.6422	118.8	17.7	735	381	0.05 ± 0.011	738	366	0.052 ± 0.012
10213X0121/HY	France	43.5563	5.6013	122.3	8.7	758	340	0.055 ± 0.012	738	366	0.049 ± 0.011
10451X0041/F	France	43.3098	5.7711	89.5	41.4	794	464	0.046 ± 0.01	773	423	0.049 ± 0.011
10444X0028/F	France	43.3016	5.7559	92.9	49.3	790	439	0.054 ± 0.012	773	423	0.053 ± 0.012
10444X0026/DA	France	43.2898	5.7099	69.8	28.2	795	516	0.029 ± 0.006	773	423	0.036 ± 0.008
10443X0291/HY	France	43.2911	5.6600	72.0	18.4	748	488	0.025 ± 0.005	773	423	0.033 ± 0.007
Kournas Lake	Greece	35.3310	24.2801	118.8	40.9	908	355	0.093 ± 0.021	900	287	0.103 ± 0.023
Vrysses	Greece	35.3764	24.2010	62.8	9.2	892	345	0.04 ± 0.009	900	287	0.045 ± 0.01
Agia Fotini	Greece	35.1396	24.5288	155.3	39.7	984	248	0.15 ± 0.033	962	397	0.115 ± 0.026
Preveli	Greece	35.1635	24.4742	86.7	24.5	940	460	0.056 ± 0.012	962	397	0.066 ± 0.015
Plakias	Greece	35.1930	24.3948	64.0	16.7	917	370	0.046 ± 0.01	962	397	0.048 ± 0.011
Lyttos	Greece	35.2279	25.3620	45.5	8.4	877	350	0.029 ± 0.007	799	347	0.025 ± 0.006
Samaria	Greece	35.4371	24.1267	29.4	14.6	876	315	0.026 ± 0.006	900	287	0.029 ± 0.006
Selena	Greece	35.2905	25.5310	29.8	10.8	847	292	0.024 ± 0.005	799	347	0.019 ± 0.004
Lentas	Greece	34.9518	24.9276	51.7	30.0	847	226	0.055 ± 0.012	770	215	0.049 ± 0.011
Rouvas	Greece	35.1381	24.9606	19.7	13.0	1011	263	0.027 ± 0.006	900	287	0.022 ± 0.005
Stylos	Greece	35.4353	24.1274	23.6	12.0	876	315	0.021 ± 0.005	900	287	0.023 ± 0.005
Kiliaris River	Greece	35.4604	24.1551	39.8	5.3	785	435	0.016 ± 0.004	900	287	0.028 ± 0.006
Zaros	Greece	35.1415	24.9065	28.0	14.0	1013	257	0.034 ± 0.008	988	282	0.032 ± 0.007
Aposelemis	Greece	35.3298	25.3333	112.4	23.9	795	415	0.054 ± 0.012	799	347	0.064 ± 0.014
Kourna Lake	Greece	35.3304	24.2753	101.6	43.3	908	355	0.085 ± 0.019	900	287	0.094 ± 0.021
Kourtaliotis	Greece	35.1548	24.4730	72.3	24.9	940	460	0.049 ± 0.011	962	397	0.058 ± 0.013

Tab. S5: Comparison of estimated annual paleo-precipitation rates from climate models for all areas with published catchment average denudation rates. For three different WorldClim paleo-climate models (Fick and Hijmans, 2017)*, paleo-precipitation values were extracted for all sampled ^{36}Cl sampling locations, averaged for each region and compared to modern precipitation rates. LGM – Last Glacial Maximum*

	model	**modern MAP [mm/a]**	**mid Holocene MAP [mm/a]**	**LGM MAP [mm/a]**	**mid Holocene /present [%]**	**LGM/ present [%]**
Israel						
	CC	552	598	545	8	-1
	MR	552	638	708	16	28
	ME	552	666	857	21	55
southern France						
	CC	769	785	757	2	-2
	MR	769	838	588	9	-24
	ME	769	781	816	2	6
Crete, Greece						
	CC	732	866	743	18	2
	MR	732	931	729	27	0
	ME	732	900	714	23	-2

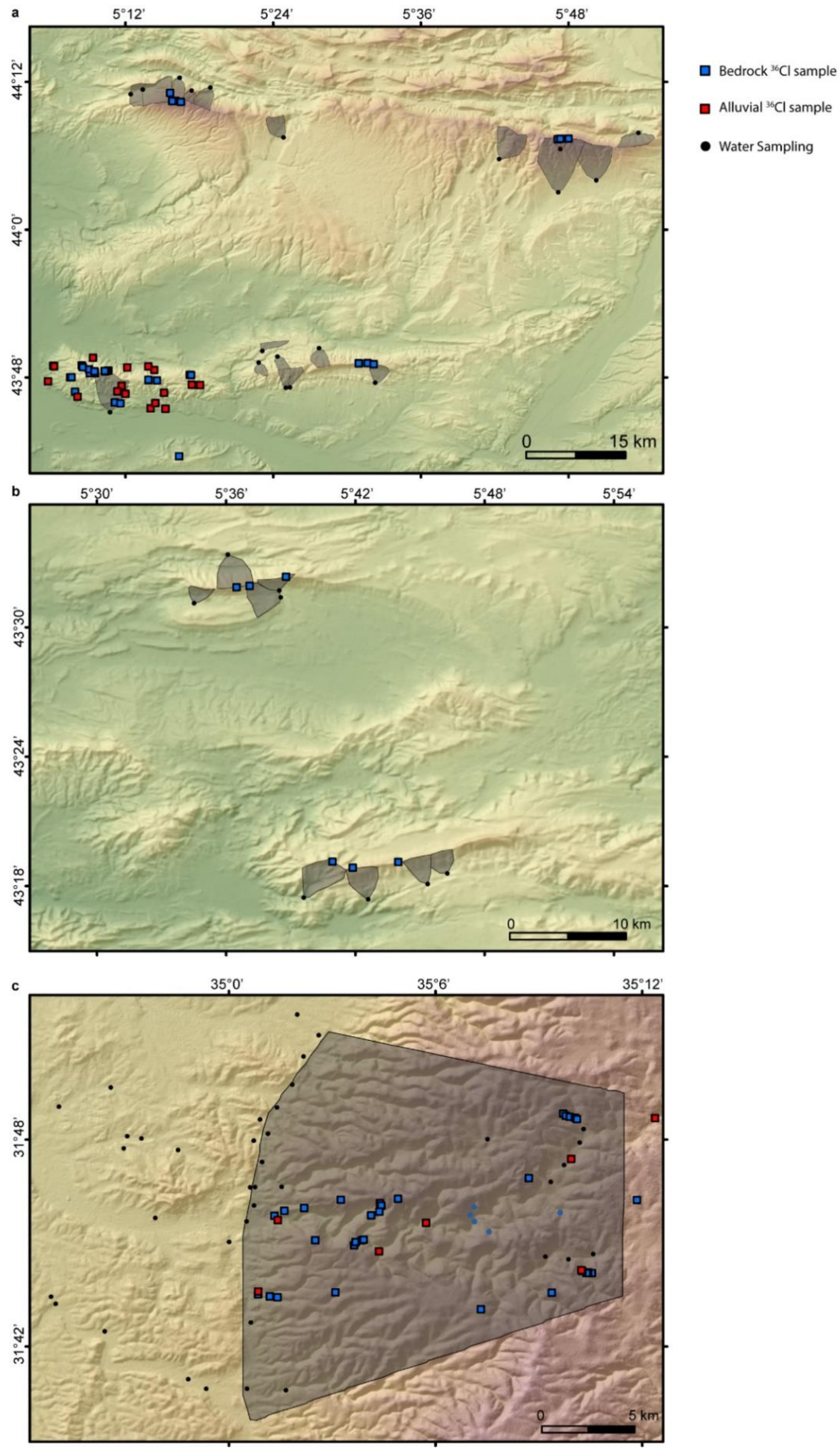

Fig. S1: Hypothetical recharge areas used to calculate the water flux required for the carbonate dissolution rate calculation for wells and springs. (a) and (b) show recharge areas for southern France, (c) for Israel, where the Western Mountain Aquifer provides the water for most wells in the coastal plain (Sheffer et al., 2010).

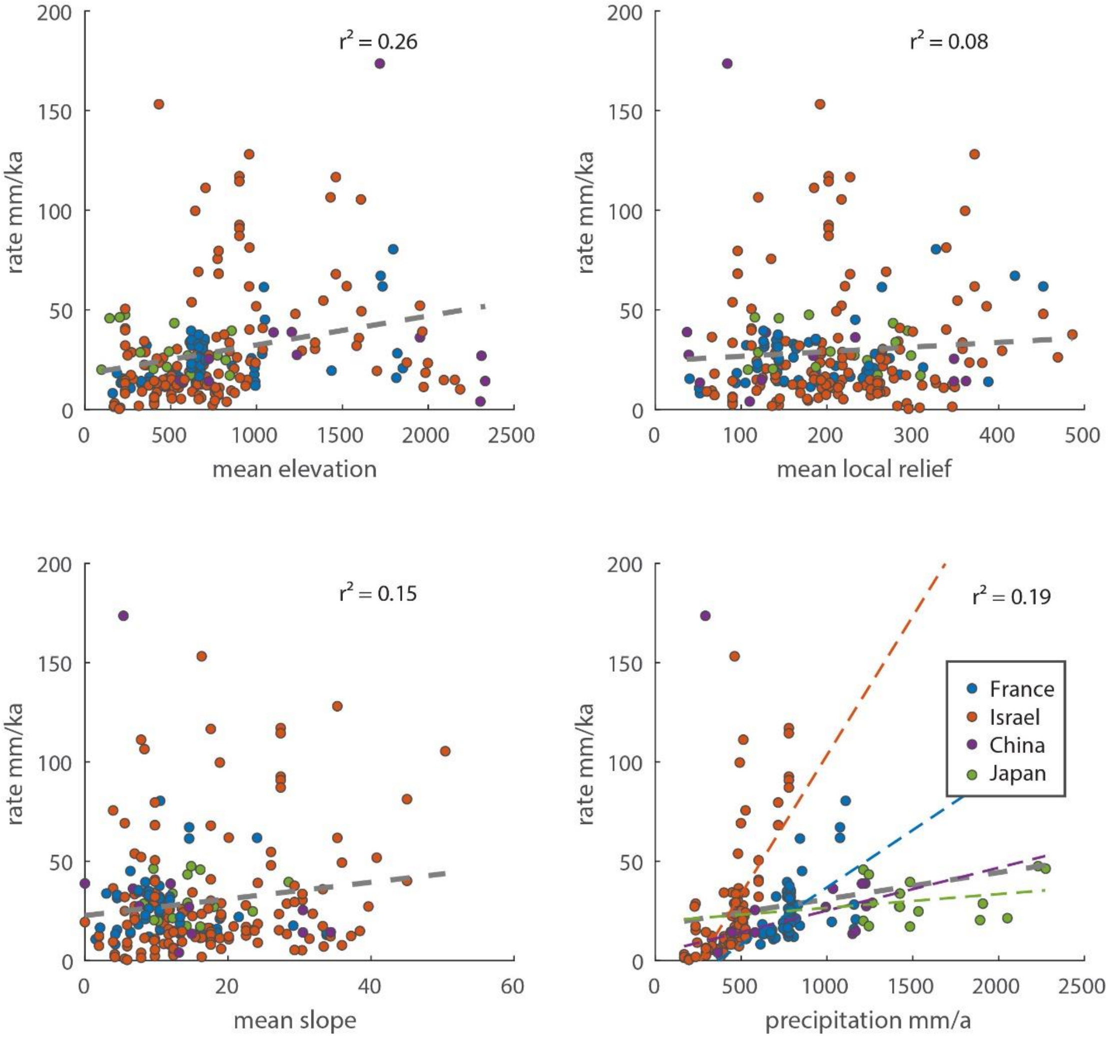

Fig. S2: Correlation between ^{36}Cl bedrock denudation rates, topographic metrics and mean annual precipitation. Colors indicate different study areas.

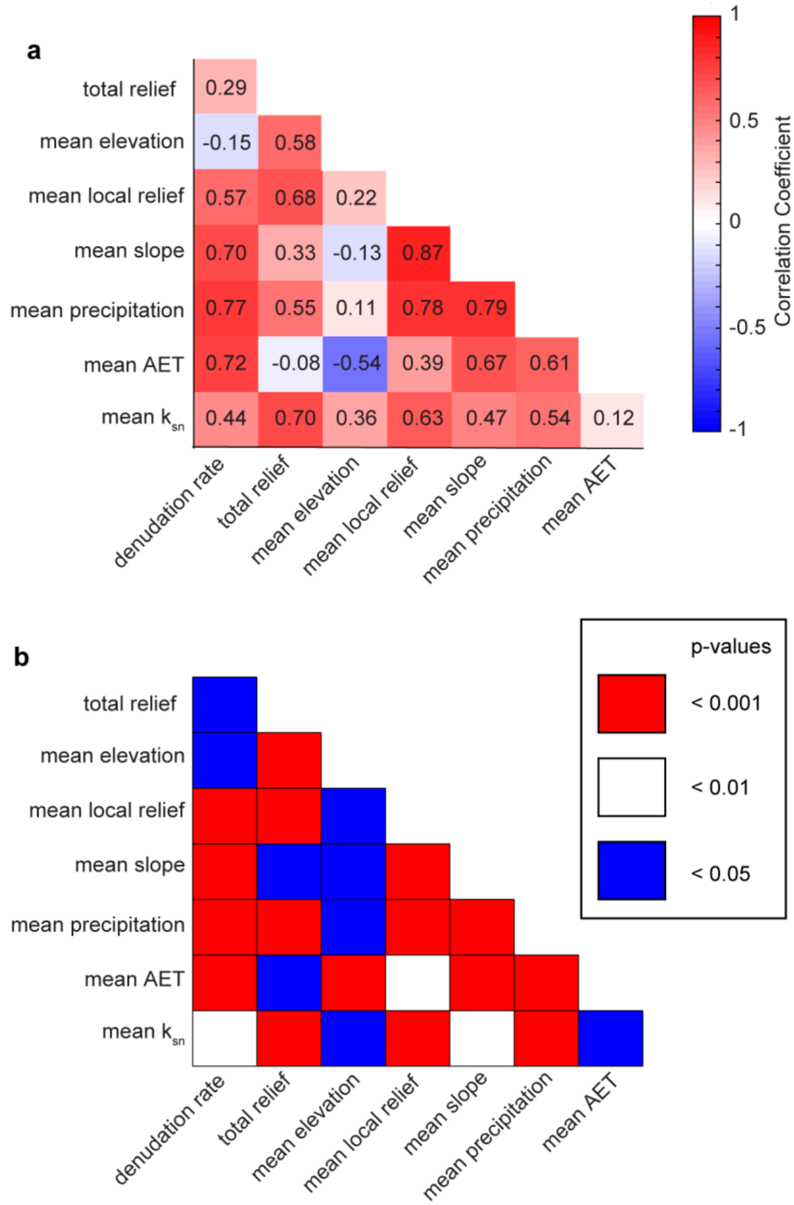

Fig. S3: (a) Correlation coefficient matrix for the data set and seven topographic and climatic metrics. Red colors indicate that most metrics are positively correlated for carbonate catchments. (b) P-value matrix for the correlation coefficient matrix in (a). The cells are colored by different significance levels.

References

Chen, S., Mulder, V.L., Martin, M.P., Walter, C., Lacoste, M., Richer-de-Forges, A.C., Saby, N.P.A., Loiseau, T., Hu, B., and Arrouays, D., 2019, Probability mapping of soil thickness by random survival forest at a national scale: Geoderma, v. 344, p. 184–194, doi:10.1016/J.GEODERMA.2019.03.016.

Fick, S.E., and Hijmans, R.J., 2017, WorldClim 2: International Journal of Climatology, v. 37, p. 4302–4315, doi:10.1002/joc.5086 T4.

Helman, D., Givati, A., and Lensky, I.M., 2015, Annual evapotranspiration retrieved from satellite vegetation indices for the eastern Mediterranean at 250 m spatial resolution: Atmospheric Chemistry and Physics, v. 15, p. 12567–12579, doi:10.5194/acp-15-12567-2015.

Helman, D., Lensky, I.M., Osem, Y., Rohatyn, S., Rotenberg, E., and Yakir, D., 2017a, A biophysical approach using water deficit factor for daily estimations of evapotranspiration and CO2 uptake in Mediterranean environments: Biogeosciences, v. 14, p. 3909–3926, doi:10.5194/bg-14-3909-2017.

Helman, D., Lensky, I.M., Yakir, D., and Osem, Y., 2017b, Forests growing under dry conditions have higher hydrological resilience to drought than do more humid forests: Global change biology, v. 23, p. 2801–2817, doi:10.1111/gcb.13551 PM - 27809388.

Helman, D., Osem, Y., Yakir, D., and Lensky, I.M., 2017c, Relationships between climate, topography, water use and productivity in two key Mediterranean forest types with different water-use strategies: Agricultural and Forest Meteorology, v. 232, p. 319–330, doi:10.1016/j.agrformet.2016.08.018.

Ott, R.F., 2022, WeCode - Weathering Corrections for denudation rates V. 1.0: GFZ Data

Services, doi:https://doi.org/10.5880/GFZ.4.6.2022.001.

Ott, R.F., Gallen, S.F., and Granger, D.E., 2022, Cosmogenic nuclide weathering biases: Corrections and potential for denudation and weathering rate measurements: Geochronology, doi:submitted.

Panagos, P., Van Liedekerke, M., Jones, A., and Montanarella, L., 2012, European Soil Data Centre: Response to European policy support and public data requirements: Land Use Policy, v. 29, p. 329–338, doi:10.1016/j.landusepol.2011.07.003.

Ryb, U., Matmon, A., Erel, Y., Haviv, I., Katz, A., Starinsky, A., Angert, A., and Team, A., 2014, Controls on denudation rates in tectonically stable Mediterranean carbonate terrain: GSA Bulletin, v. 126, p. 553–568, doi:10.1130/B30886.1.

Schwanghart, W., and Scherler, 2014, Short Communication: TopoToolbox 2 – MATLAB-based software for topographic analysis and modeling in Earth surface sciences: Earth Surface Dynamics, v. 2, p. 1–7, doi:10.5194/esurf-2-1-2014.

Sheffer, N.A., Dafny, E., Gvirtzman, H., Navon, S., Frumkin, A., and Morin, E., 2010, Hydrometeorological daily recharge assessment model (DREAM) for the Western Mountain Aquifer, Israel: Model application and effects of temporal patterns: Water Resources Research, v. 46, p. 251, doi:10.1029/2008WR007607.

Stallard, R.F., and Edmond, J.M., 1981, Geochemistry of the Amazon: J. Geophys. Res., v. 86, p. 9844, doi:10.1029/JC086iC10p09844.